

THERMAL DETECTION OF PARAMAGNETIC RESONANCE

W. S. MOORE

*Department of Physics, University of Nottingham, University Park,
Nottingham NG7 2RD, UK*

ABSTRACT

Recently Gorter's original technique for the detection of paramagnetic resonance by the rise in specimen temperature following the absorption of resonant electromagnetic energy has been successfully revived by Solomon and utilized in a series of experiments on spin-dependent effects in solids. We have made a study of the use of thermally detected EPR to examine paramagnetic centres in solids. We have found the method to be very generally applicable but to be particularly useful for strongly coupled non-Kramers ions, which have enormous resonance linewidths and very short spin-lattice relaxation times. It appears in these cases that it is the electric field of the incident electromagnetic radiation which interacts, via optic-type lattice displacements, with the orbital part of the paramagnetic impurity wave functions, thereby causing transitions. The selection rules are thus similar to those for acoustic paramagnetic resonance absorption.

The experimental techniques that are used will be described and the different types of experiment possible will be illustrated by results for the thermally detected EPR of a variety of paramagnetic ions in different lattices. The information to be gained by this method is compared with that obtained from conventional EPR and APR.

I. INTRODUCTION

Gorter¹ proposed a long time ago that the resonant absorption of electromagnetic energy by paramagnetic spin systems could be observed by the resulting rise in temperature of a thermally isolated sample. The logic of this proposal is appealing when insulating samples are considered, because there is then no limit to the electromagnetic fields that may be applied to detect weak resonances, i.e. small signals are not superimposed on a large steady signal present at the detector as in conventional spectroscopy. It is surprising that the method has not been used more widely throughout the electromagnetic spectrum. It has, however, been taken up with considerable success by Schmidt and Solomon^{2, 3} and developed for the case where the resistance of an electrically conducting sample acts as the sample's own temperature sensor. The possibilities of thermally detected electron paramagnetic resonance (TD-EPR) to investigate impurities in insulating lattices have been explored by Moore and Al-Sharbaty⁴ (to be referred to as E1) and by Moore, Bates and Al-Sharbaty⁵ (to be referred to as E2). In E1 preliminary details are given of TD-EPR methods used to study Kramers ion impurities in MgO.

In E2 it is shown that a new mechanism allows electric field induced EPR (EF-EPR) for non-Kramers ions in the non-centrosymmetric sites of solids. Details of the current experimental arrangement used to study TD-EPR are given in Section III, and a review of the information so far obtained by this method is given in Section IV.

II. THEORY

It is stated in E1 and shown by Schmidt and Solomon² that, for N spins, the power Π given to the lattice by the spin-lattice relaxation with time T_1 of pairs of levels with energy separation $\hbar\omega$ at temperature T is given by:

$$\Pi = \left(\frac{P}{P + P_s} \right) \left(f(T) \right) \left(\frac{N\hbar\omega}{T_1} \right) \left(\frac{S(S+1)}{3} \right) \quad (1)$$

The first bracket is the saturation factor, P being the incident electromagnetic power and P_s the power required to reduce the population difference to one-half its equilibrium value. The second bracket is the Boltzmann factor for the pair of levels involved. The third bracket is the power expected if all N spins are saturated ($P \gg P_s$), and the fourth arises from the detailed calculation for spin S . There are two important limiting cases.

Saturation ($P \gg P_s$)

$$\Pi_s \propto \frac{N \cdot f(T)}{T_1} \quad (2)$$

This is the normal situation with Kramers ions, which tend to be weakly coupled to the lattice, especially at very low temperatures.

Far from Saturation ($P \ll P_s$)

$$\Pi_u \propto Q \cdot P \cdot T_2 \cdot N \cdot f(T) \quad (3)$$

Q is the quality factor of a cavity fed with microwave power P and T_2 is the reciprocal linewidth for the homogeneous EPR line. Π_u is independent of T_1 , because $P_s \propto 1/T_1 T_2$. This is the normal situation with non-Kramers ions, which tend to be strongly coupled to the lattice, even at very low temperatures.

The power Π from an impurity spin system heats up the lattice of the host solid and also a quartz rod and a thermometer (see Section III). The details are given in *Figure 1*, as are the various time constants associated with the approach to equilibrium of the various parts of the system. To obtain TD-EPR spectra, the magnetic field is varied as for normal EPR and the temperature T of the lattice plus rod plus thermometer is displayed. The rate of field sweep is such that the absorption lines of interest are traversed in a time long compared with τ (*Figure 1*), the limiting response time, usually about 1 s. All experiments so far have been done in the liquid helium temperature range, where the very small specific heat of the sample lattice and the quartz rod not only lead to very large temperature rises for small Π , typically 0.1 K/ μ W, but also lead to a short time constant even when the heat leak is very small.

THERMAL DETECTION OF PARAMAGNETIC RESONANCE

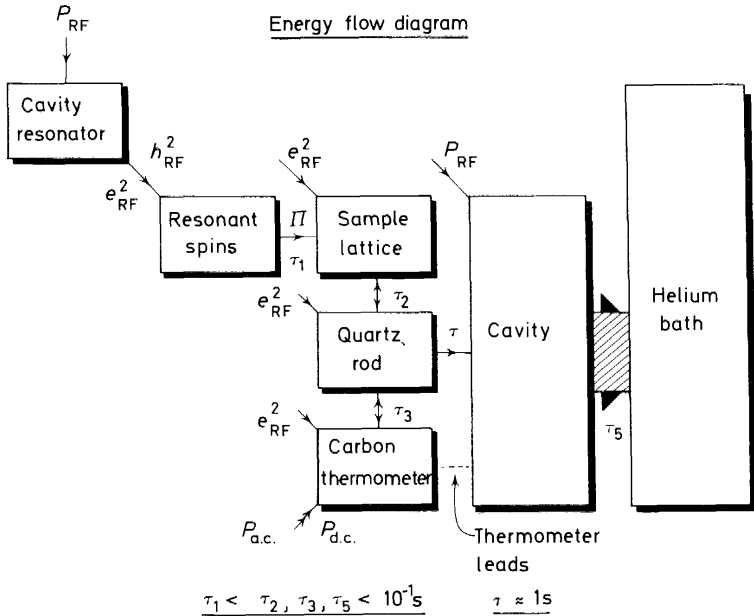


Figure 1. Schematic diagram showing the effects of radio-frequency magnetic fields h_{RF} and electric fields e_{RF} in heating various component parts of the cavity of Figure 2. $P_{a.c.}$ is the a.c. power used to measure the carbon thermometer resistance and $P_{d.c.}$ is the d.c. power used to calibrate the system. The τ s are thermal time constants

Conventional EPR transitions ($\Delta J'_z = 1$) are caused by the radio-frequency magnetic field h_{RF} when the specimens are located near the end face of the cavity (Figure 2). EF-EPR transitions ($\Delta J'_z = 0, 1, 2$) are observed with the specimen in the middle of the cavity, where the radio-frequency electric field e_{RF} is maximum. The mechanism in the latter case is explained in E2, and is briefly that e_{RF} causes dynamic optic-type displacements of the lattice, which in the case of a non-centrosymmetric site leads to transitions of the central magnetic ion, in the same way as do the dynamic displacements of ultrasound in an APR experiment.

III. EXPERIMENTAL DETAILS

The use of a microwave cavity for TD-EPR is not necessary but, as equations (2) and (3) show, its use results in larger signals Π_u and allows saturation of weakly coupled ions with very low incident microwave power. We have used an evacuable cylindrical TE_{111} cavity made in three parts, shown schematically in Figure 2. Extruded indium ring vacuum seals are used, which successfully exclude liquid helium, even below the λ -point. The upper seal is made along the line of zero wall-current for the TE_{111} mode, leading to a loaded Q of the resonator at 4 K of about 2×10^4 . Longer single-crystal quartz rods are now used than previously described in E1 and this ensures that there is no direct heating of the thermometer by e_{RF} . Any heat detected by the

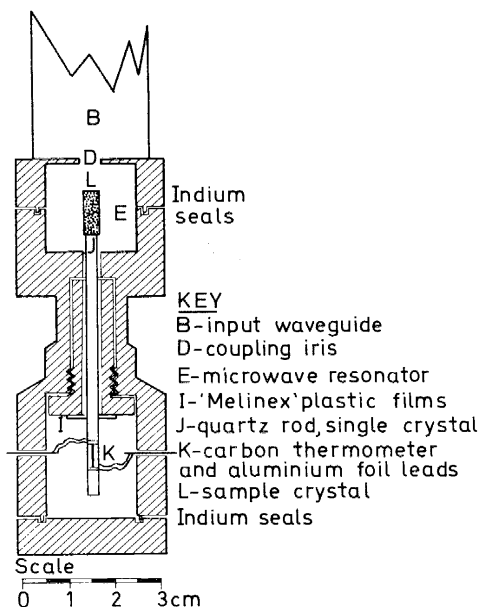


Figure 2. Schematic diagram of the solid copper TE_{111} cavity used for TD-EPR measurements. The three cylindrical parts bolt together, and the resonant frequency is ~ 11 GHz

carbon film thermometer comes from the specimen only, since we know the small amount by which the end of the quartz rod in the cavity is heated directly by e_{RF} . We still know little about τ_1 (Figure 1), the time it takes the phonon spectrum with a peak at ω to revert to a black-body spectrum. τ_2 has been found to exceed τ if a fused silica rod is used in place of a single crystal. τ_3 can become very long if the carbon film thermometer accidentally becomes detached from the quartz rod. This is easily noticed, however, from the enormous temperature rises that are observed when a d.c. current is passed through the thermometer while its resistance is being measured by an a.c. bridge. τ_5 is always very short, since the copper cavity is immersed directly in liquid helium. We have found that in the earlier experiments reported in E1 and E2 the dominant time constant was not always due to the plastic strip quartz rod supports, but was due either to the aluminium foil connections to the thermometer or more often to thermal conduction through helium gas in the cavity. At pressures of around 10^{-4} Torr in the cavity we have observed a very sharply field-dependent gas breakdown phenomenon. This we attribute to cyclotron resonance assisted ionization of the helium gas from the low-threshold microwave power needed (1 mW) and since it occurs at a magnetic field such that the g -value is two. This effect was first observed by Lax⁶ and can be seen in Figure 7. The use of pressures lower than 10^{-5} Torr removes this effect and also provides adequate thermal insulation.

No attempt has so far been made to improve the sensitivity (1 mK at 4 K) of the carbon film thermometer and associated a.c. bridge, since it has proved adequate to detect strongly coupled ionic substitutional impurities down to atomic concentrations of 10^{-8} (see Section IV).

THERMAL DETECTION OF PARAMAGNETIC RESONANCE

The single-crystal Al_2O_3 specimens which we have been examining are often accurately ground cylinders, with the trigonal axis perpendicular to the cylinder axis. We have found that the introduction of such a specimen along the cavity axis removes the degeneracy of the two perpendicularly polarized

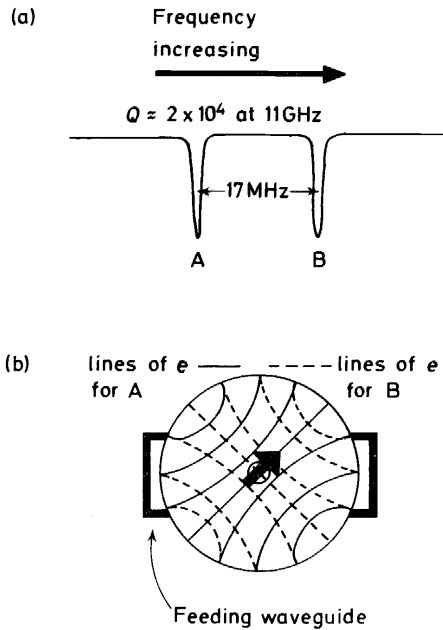


Figure 3. (a) The reflected power from the resonator of Figure 2, showing the two normal modes A, B caused by the anisotropic specimen. (b) The radio-frequency electric field lines of the cylindrical TE_{111} cavity associated with the two modes. The arrow represents the direction of the trigonal axis of the cylindrical specimen which is causing the frequency difference between modes A and B

TE_{111} modes. There are then two possible normal modes for the cavity, separated by a few tens of megahertz, whose planes of polarization are exactly parallel and perpendicular to the trigonal axis of the crystal^{7, 8}. If the crystal is rotated about its axis until the trigonal axis makes an angle of 45° with the input waveguide polarization direction, then these modes become equally coupled to the input waveguide. A typical reflected power versus frequency curve for the resonator under these conditions is shown in Figure 3. Use is made of these two modes to enable TD-EPR spectra to be obtained with radio-frequency fields e_{RF} and h_{RF} accurately parallel or perpendicular to crystalline axes, simply by adjustment of the microwave frequency from one mode to the other.

In use, the specimen and quartz rod in the cavity of Figure 2 take about an hour to cool via the small heat leak through the aluminium foil leads from 70 K to 4 K after the cavity has been immersed in liquid helium. This reflects the T^3 variation in specific heat, and its effect on the thermal time constant.

IV. EXPERIMENTAL RESULTS

A. Ions in MgO

In E1 details are given of the measurements made on both Cr-doped and nominally pure MgO. The TD-EPR spectra of Fe^{2+} , Fe^{3+} , Mn^{2+} and Cr^{3+} in various sites were observed simultaneously with their conventional EPR spectrum, with all transitions being caused by h_{RF} . In Cr-doped MgO an additional new line of width about 1 kG centred on $g = 2$ was obtained and ascribed to Cr^{3+} at sites which are randomly compensated. It appears that most of the ions are in such sites. Conventional EPR spectral recordings, especially where the derivative is detected by magnetic field modulation, would have extreme difficulty in detecting this absorption. The same was found for nominally pure MgO, namely that there was a broad resonance centred on $g = 2$ which was ascribed in that case to Fe^{3+} in randomly compensated sites. In both these cases by 'random compensation' we mean that the charge compensation is long-range and that no particular ion can be said to compensate Cr^{3+} or Fe^{3+} , respectively, unlike the known discrete lines found by Wertz and Auzins⁹, where, for instance, Cr^{3+} is sometimes closely associated with a cation vacancy in the second-nearest-neighbour position along a cube direction. TD-EPR is less sensitive than conventional EPR for the narrow-line spectra of Fe^{3+} , Cr^{3+} and Mn^{2+} where Π_s (equation 2) is limited by T_1 . It is, however, far more sensitive than conventional EPR for detecting broad lines such as those mentioned above and Fe^{2+} . There is even more advantage to be gained if the broad-line impurities have a short T_1 , as more microwave power can be used before saturation limits the observed temperature rise.

B. Ions in Al_2O_3

Fe^{2+} , Fe^{3+} . In E2 the TD-EPR spectra of Fe^{3+} and Fe^{2+} ions were shown for excitation by both h_{RF} and e_{RF} . When h_{RF} is used, the saturated Fe^{3+} spectrum dominates the very weak Fe^{2+} spectrum. When e_{RF} is used, the situation is reversed, and the Fe^{2+} spectrum, still unsaturated, dominates the very weak Fe^{3+} spectrum. Both ways of exciting the spectrum are useful. When h_{RF} is used, the change in height of the dominant saturated Fe^{3+} thermal signals is very sensitive to changes in T_1 (equation 2), owing to cross-relaxation with Fe^{2+} ions. This effect has been used to estimate the strength of the Fe^{2+} - Fe^{3+} coupling and has led to a new proposed mechanism to explain the coupling of a Kramers ion such as Fe^{3+} to a non-Kramers ion such as Fe^{2+} . Such coupling cannot be magnetic, because $g_{\perp} = 0$ for Fe^{2+} , and so it was supposed that it was caused by the electric fields at Fe^{2+} sites arising from the changing electric quadrupole moment of neighbouring Fe^{3+} ions when they make magnetic dipole transitions (Bates *et al.*¹⁰). EF-EPR, on the other hand, gives very similar spectra to APR and allows a detailed study of the Fe^{2+} ion's line shape and position, leading to a determination of the Hamiltonian parameters describing its interaction with lattice strains and applied fields. As an example of the sensitivity of the method, Figure 4 shows the fit of the Fe^{2+} asymmetric TD line to the function $\exp[-(H_0 - H)]$ when the magnetic field H is less than the high-field cut-off H_0 , and when

THERMAL DETECTION OF PARAMAGNETIC RESONANCE

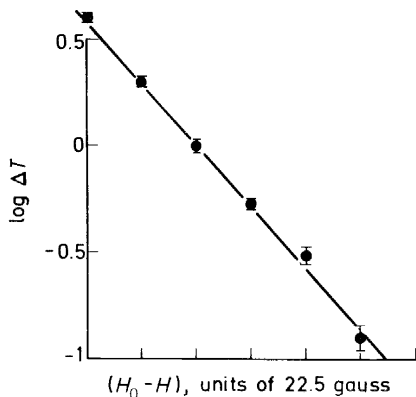


Figure 4. The fit of the observed TD-EPR line of Fe^{2+} ions in Al_2O_3 to the line shape function $\exp[-(H_0 - H)]$, where $H < H_0$

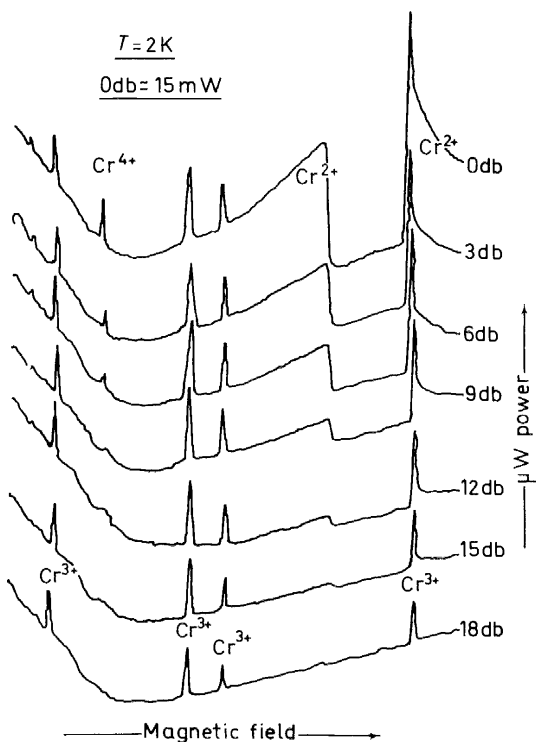


Figure 5. TD-EPR spectra at different microwave power levels excited by both h_{RF} and e_{RF} for γ -irradiated Cr-doped Al_2O_3 (ruby) crystals

H is parallel to the trigonal axis. This spectrum was obtained with a Fe^{2+} concentration of a few p.p.m. This line shape is thought to be due to a Gaussian distribution of strains centred on zero, which have only a second-order effect on the energy of the $\Delta J_z = 2$ transition of Fe^{2+} which is observed. Thus, TD-EPR can give detailed information on the strain type and distribution in a lattice by studying its effect on the spectrum of strongly coupled impurities present in very small concentrations. This ability is more strikingly obvious from the spectra of Ni^{3+} in Figure 7, to be discussed later.

Cr^{2+} , Cr^{3+} , Cr^{4+} , Cr^{5+} . Figure 5 shows a typical set of TD spectra excited by both h_{RF} and e_{RF} taken at different power levels for a γ -irradiated Cr-doped Al_2O_3 specimen. This illustrates equations 2 and 3, in that the

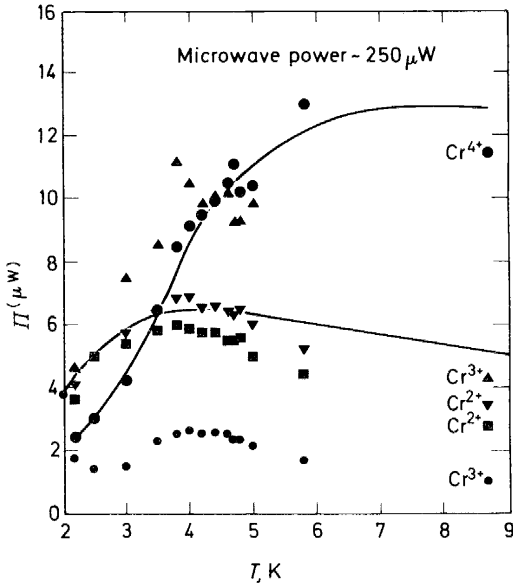


Figure 6. Π (equation 1), the resonant power absorbed by various ions in Al_2O_3 , as a function of temperature at constant microwave power

signals from Cr^{3+} can be seen to be saturated at all the microwave power levels, whereas neither Cr^{2+} nor Cr^{4+} shows any signs of saturation up to 15 mW incident. If such measurements are made at a series of temperatures, then Figure 6 results. Here can be seen the unsaturated signals Π_u from Cr^{4+} and Cr^{2+} and the saturated signal Π_s from Cr^{3+} as a function of temperature, measured at constant microwave power. The variation in Π_u reflects the Boltzmann factors for Cr^{2+} and Cr^{4+} . The diagram shows the Boltzmann factor for a pair of levels at 7 cm^{-1} in the case of Cr^{4+} ¹¹ and a Boltzmann factor based on the theory of Bates, Jaussaud and Smith¹² for Cr^{2+} . In the case of Π_s for Cr^{3+} , since the transition arises from the ground state, the Boltzmann factor is $\propto 1/T$. Thus, Π_s should be constant, since $T_1 T$ is a constant if T_1 is dominated

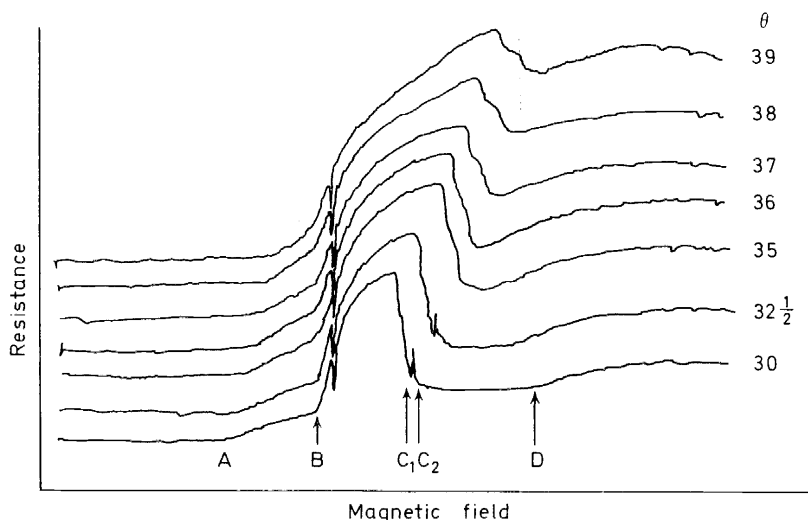


Figure 7. The TD-EPR spectra of Ni^{3+} ions in Al_2O_3 single crystals. θ is the angle that the magnetic field makes with the trigonal axis. Features A, B and D are slope discontinuities, and C_1, C_2 are the two steepest points on the edge. The narrow features near B (visible on all curves) and near C_1, C_2 visible on curves $\theta = 30, 32\frac{1}{2}$ are due to cyclotron resonance assisted gas breakdown, as explained in the text

by the direct one-phonon process. In fact, because the Cr^{3+} ions are relaxed by the Cr^{2+} ions¹³ via the coupling discussed above for the $\text{Fe}^{2+}-\text{Fe}^{3+}$ case, H_s for Cr^{3+} varies with the same Boltzmann factor as Cr^{2+} .

Recent experiments on the same Al_2O_3 sample doped with both magnesium and chromium which has been studied by Brown¹⁴ have shown what we believe to be the first new spectrum to be obtained by TD EF-EPR, namely that of the ion Cr^{5+} . Although the experiments and their analysis are not yet complete, the g -value of 1.69 is consistent with its position in the isoelectronic series $\text{Ti}^{3+}, \text{V}^{4+}, \text{Cr}^{5+}$.

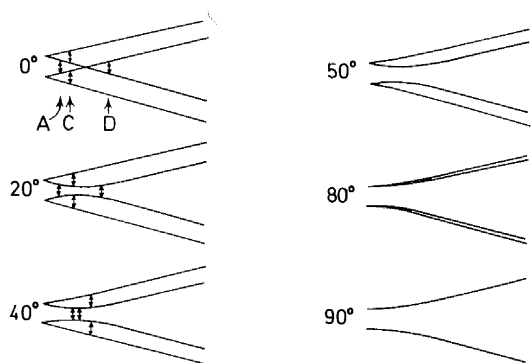


Figure 8. The energy levels as a function of magnetic field for various angles θ of the magnetic field to the Z axis for a 2E ground state and the Hamiltonian shown

Ni^{3+} . Figure 7 shows typical TD EF-EPR spectra from Ni^{3+} -doped Al_2O_3 . These are very similar to the previous APR results of Abou-Ghantous¹⁵. The strange line shapes are due to the effect of the detailed distribution and type of the internal strains in the crystal. The relatively insignificant features A, C_1 , C_2 , D are thought to be characteristic of the unstrained Ni^{3+} ion, while feature B is thought to arise from highly strained sites. The ground state of Ni^{3+} is 2E , and Figure 8 shows the energy level diagrams obtained for the unstrained Hamiltonian

$$\mathcal{H} = g\beta\mathbf{H}\cdot\mathbf{S} + \Lambda T_z S_z \quad (4)$$

where $\mathbf{S} = \frac{1}{2}$, and $\mathbf{T} = \frac{1}{2}$ represents the twofold orbital degeneracy. The transitions giving rise to A, C_1 , C_2 and D are shown, and B is thought to be due to transitions within the two doublets when they are well separated by large strains and behave like two free spins of $\frac{1}{2}$. The Hamiltonian of equation (4) is exactly soluble for all angles θ of the magnetic field to the trigonal axis. This yields $1/h^2 = (\cos^2 \theta - \rho^2)/(1 - \rho^2)$ for features C_1 and C_2 and $h\rho = \cos \theta \pm (\rho^2 - \sin^2 \theta)^{\frac{1}{2}}$ for features A and D, where $\rho = 2\hbar\omega/\Lambda$.

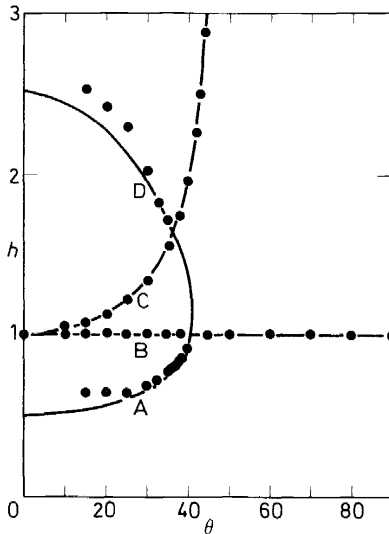


Figure 9. The theoretical (solid line) and experimental (dots) isofrequency plot for Ni^{3+} measured at 9.35 GHz. $h = H/H_0$ and $H_0 = \hbar\omega/g\beta$

$h = H/H_0$ and $H_0 = \hbar\omega/g\beta$. These variations are shown in Figure 9 along with the measured values taken from curves such as those of Figure 7. A zero field splitting $\Lambda/2 = 0.470 \pm 0.005 \text{ cm}^{-1}$ and $g = 2.150 \pm 0.005$ are obtained. Full details of these calculations and experiments will be published shortly¹⁵. It can be seen that it is the detailed combination of strain, transition probability and Boltzmann factor which gives rise to the observed line shape in this case.

V. CONCLUSIONS

We have shown in this brief review of the experimental data obtained that a great deal of useful information can be obtained by TD-EPR measurements. The broad lines from weakly coupled Kramers ions and strongly coupled non-Kramers ions can be detected in the same experiment with greater sensitivity than can be obtained in separate conventional EPR or APR experiments. In addition, the coupling between different ionic species can easily be studied, as can saturation phenomena at high incident microwave power levels. EF-EPR, however, seems to be possible only for ions at sites lacking inversion symmetry. Preliminary results indicate also that a detailed knowledge of the strain distribution in a solid can be obtained from the effect of the strain on the EF-EPR of strongly coupled ions. Further experiments on a variety of ions in organic and inorganic crystalline and amorphous host materials are either planned or in progress.

VI. ACKNOWLEDGEMENTS

I should like gratefully to acknowledge the experimental assistance of Tahir Al-Sharbati and the work reported in his Ph.D. thesis. I should also like to thank many colleagues for fruitful discussions and collaboration on numerous occasions, particularly Professor K. W. H. Stevens, Dr C. A. Bates, Dr J. R. Fletcher, Michel Abou-Ghantous and Madame A.-M. Vasson.

REFERENCES

- ¹ C. J. Gorter, *Physica*, **3**, 995 (1936).
- ² J. Schmidt and I. Solomon, *J. Appl. Phys.* **37**, 3719 (1966).
- ³ I. Solomon, *Physics Bulletin*, **23**, 451 (1972).
- ⁴ W. S. Moore and T. M. Al-Sharbati, *J. Phys. D: Applied Phys.* **6**, 367 (1973).
- ⁵ W. S. Moore, C. A. Bates and T. M. Al-Sharbati, *J. Phys. C: Solid State Phys.* **6**, L209 (1973).
- ⁶ B. Lax, W. P. Allis and S. C. Brown, *J. Appl. Phys.* **21**, 1297 (1950).
- ⁷ W. S. Moore, *Rev. Sci. Instrum.* **44**, 158 (1973).
- ⁸ I. A. Clark and W. S. Moore to be published.
- ⁹ J. E. Wertz and P. Auzins, *Phys. Rev.* **106**, 484 (1957).
- ¹⁰ C. A. Bates, W. S. Moore, T. M. Al-Sharbati and P. Steggles; and A. Gavaix, A.-M. Vasson and A. Vasson, *J. Phys. C: Solid State Phys.* **7**, L83 (1974).
- ¹¹ R. H. Hoskins and B. H. Soffer, *Phys. Rev.* **133A**, 490 (1964).
- ¹² C. A. Bates, P. C. Jaussaud and W. Smith, *J. Phys. C: Solid State Phys.* **6**, 898 (1973).
- ¹³ M. A. Brown, L. J. Challis, W. S. Moore, D. L. Waldorf and T. S. Yalcin, *J. Phys. C: Solid State Phys.* **6**, 1063 (1973).
- ¹⁴ M. A. Brown, *J. Phys. C: Solid State Phys.* **6**, 642 (1973).
- ¹⁵ M. Abou-Ghantous, C. A. Bates, I. A. Clark, J. R. Fletcher, P. C. Jaussaud and W. S. Moore, *J. Phys. C: Solid State Phys.* **7**, 2707 (1974) and *Phys. Rev. Letters*, **33**, 530 (1974).